Supporting Information

Lowing the melting point of ZIF via anion competing effect in MOF hybrid glass

Zipeng Liu,[a,b,c] Chengwei Gao,*[a,b,c] Linling Tan,[a,b,c] Shiliang Kang,[a,b,c] Qing Jiao,[a,b,c] Wenjie Xie,[d] Gang Zhou,[e] Changgui Lin,[a,b,c]

[a] Laboratory of Infrared Materials and Devices, The Research Institute of Advanced Technologies, Ningbo University, Ningbo, 315211, China
[b] Zhejiang Key Laboratory of Advanced Optical Functional Materials and Devices, Ningbo University, Ningbo, 315211, China
[c] Engineering Research Centre for Advanced Infrared Photoelectric Materials and Devices of Zhejiang Province, Ningbo University, Ningbo, 315211, China
[d] Department of Materials and Earth Sciences, Technical University of Darmstadt, 64287 Darmstadt, Germany
[e] Ningbo Sunny Infrared Optics Technologies Co, Yuyao, 315400, P.R. China

***Corresponding authors:** Chengwei Gao, E-mail: gaochengwei@nbu.edu.cn

Table S1. Comparison of T_g, T_m and GFA of typical glass systems

Type	Component	T_g (°C)	T_m (°C)	GFA	Reference
MOF glass	ZIF-62	330	420	0.84	1
	TIF-4	350	440	0.87	2
	ZIF-4	583	304	0.67	1
Oxide glass	SiO_2	1175	1713	0.73	3
	B_2O_3	267	450	0.75	3
Chalcogenide glass	As_2S_3	185	310	0.78	4
	GeS_2	492	840	0.68	4
	$Te_{85}Ge_{15}$	230	401	0.57	5
	$Te_{75}Ge_{25}$	205.5	363	0.57	5
Polymer glass	CPs	29	41.5	0.70	6
halide salt glass	$ZnBr_2$	122	385	0.59	7
	$ZnCl_2$	102.5	318	0.64	8
MOF hybrid glasses	$(ZIF\text{-}62)_{0.9}(ZnBr_2)_{0.1}$	161	**216**	**0.89**	**This work**
	$(ZIF\text{-}62)_{0.7}(ZnBr_2)_{0.3}$	154	**196**	**0.91**	
	$(ZIF\text{-}62)_{0.5}(ZnBr_2)_{0.5}$	142	**169**	**0.94**	
	$(ZIF\text{-}62)_{0.3}(ZnBr_2)_{0.7}$	76.5	**141**	**0.84**	
	$(ZIF\text{-}62)_{0.2}(ZnBr_2)_{0.8}$	71	**133**	**0.85**	
	$(ZIF\text{-}62)_{0.1}(ZnBr_2)_{0.9}$	-	**106**	**-**	

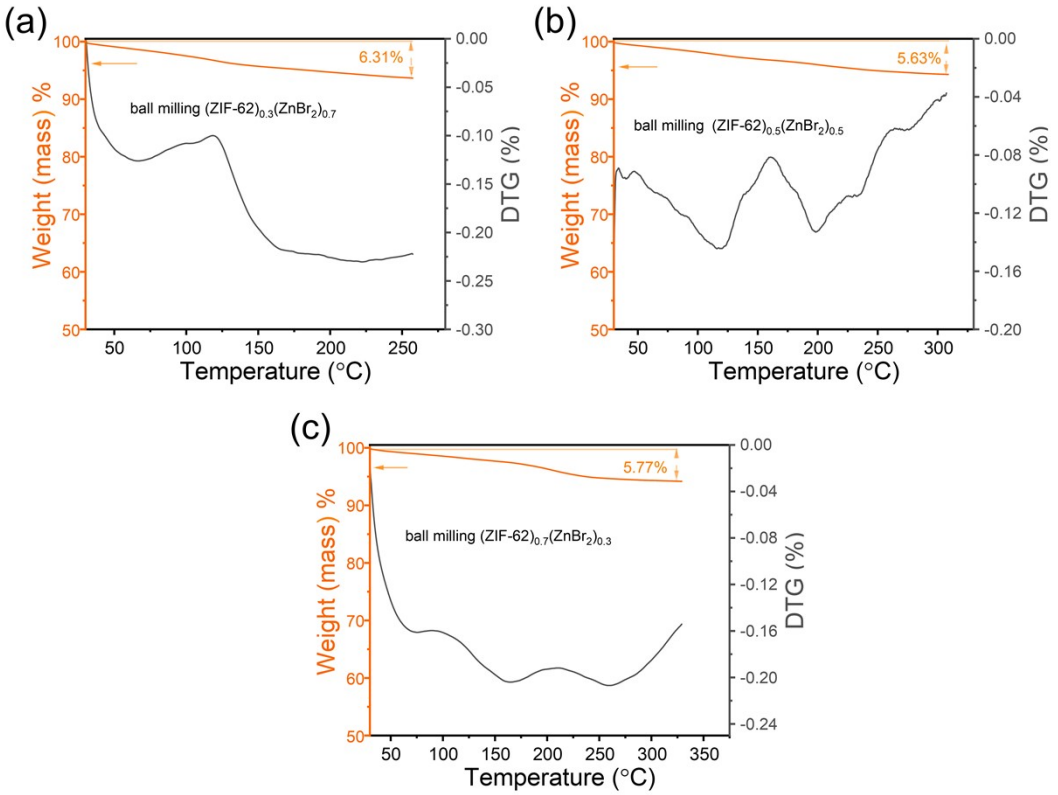

Figure S1. Thermogravimetric (TG) and derivative thermogravimetric (DTG) curves of precursor mixtures with (a) x=0.3, (b) x=0.5, and (c) x=0.7. The TG curves (orange) represent the mass change, while the DTG curves (black) indicate the corresponding rate of mass loss as a function of temperature.

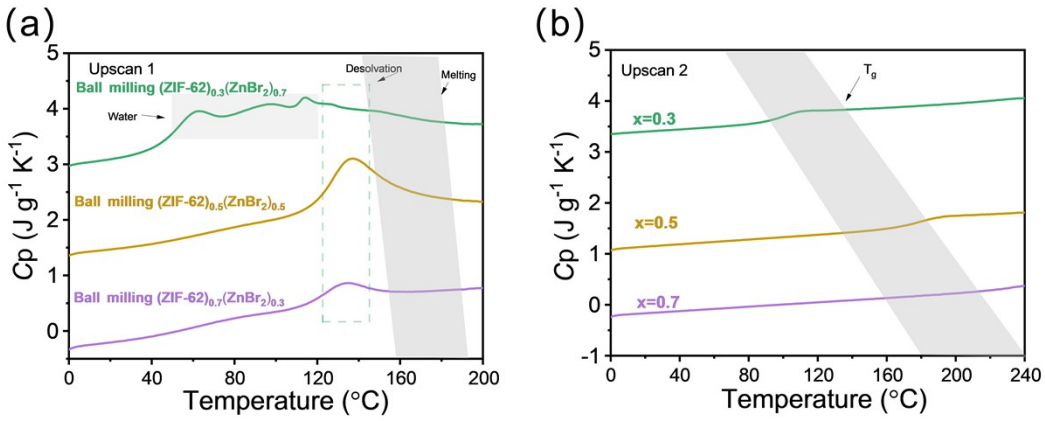

Figure S2. DSC curves of ball-milled $(ZIF\text{-}62)_{1-x}(ZnBr_2)_x$. (a) first heating scan showing desorption and melting processes; (b) second heating scan highlighting the Tg and its dependence on ZnBr2 content.

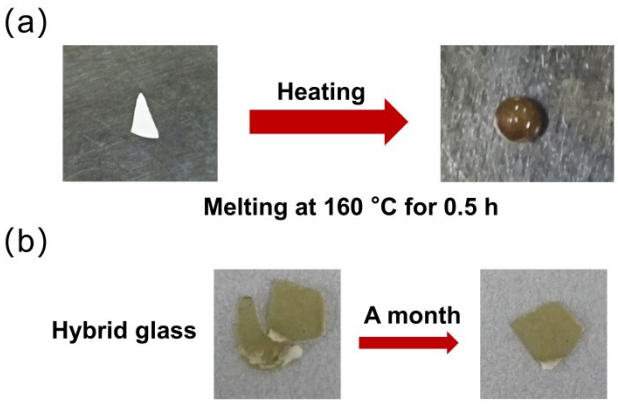

Figure S3. (a) Photographic image of the melting process of $(ZIF\text{-}62)_{0.5}(ZnBr_2)_{0.5}$ hybrid glass precursor, where melting occurs after 0.5h heating at 160 °C with white solid tablets; (b) Stability test of the prepared hybrid glass, showing no significant crystallization or decomposition after one month storage under indoor conditions

(a)

Element / Sample	Br	Zn	C	N
x=0.3	12.07%	11.56%	60.51%	15.87%
x=0.5	5.33%	9.78%	66.19%	19.12%
x=0.7	2.98%	9.47%	67.09%	21.49%

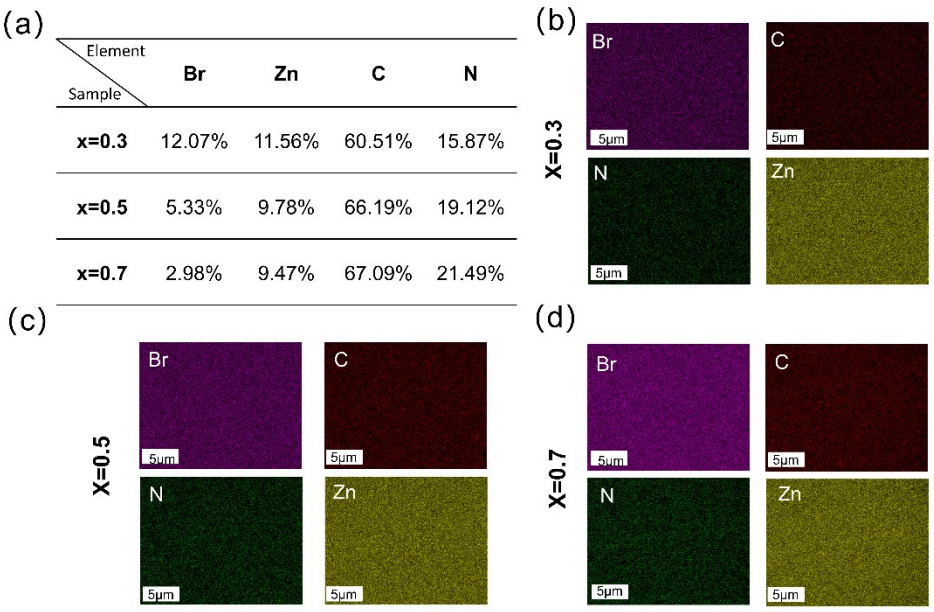

Figure S4. (a) Elemental composition (at.%) of $(ZIF\text{-}62)_{1-x}(ZnBr_2)_x$ hybrid glasses with x = 0.3, 0.5, and 0.7, determined by energy dispersive X-ray spectroscopy (EDS). (b-d) Corresponding EDS elemental mapping images of Br, C, N, and Zn for the samples with x = 0.3, 0.5, and 0.7, respectively, demonstrating the homogeneous distribution of all elements at the micrometer scale. The scale bar is 5 μm.

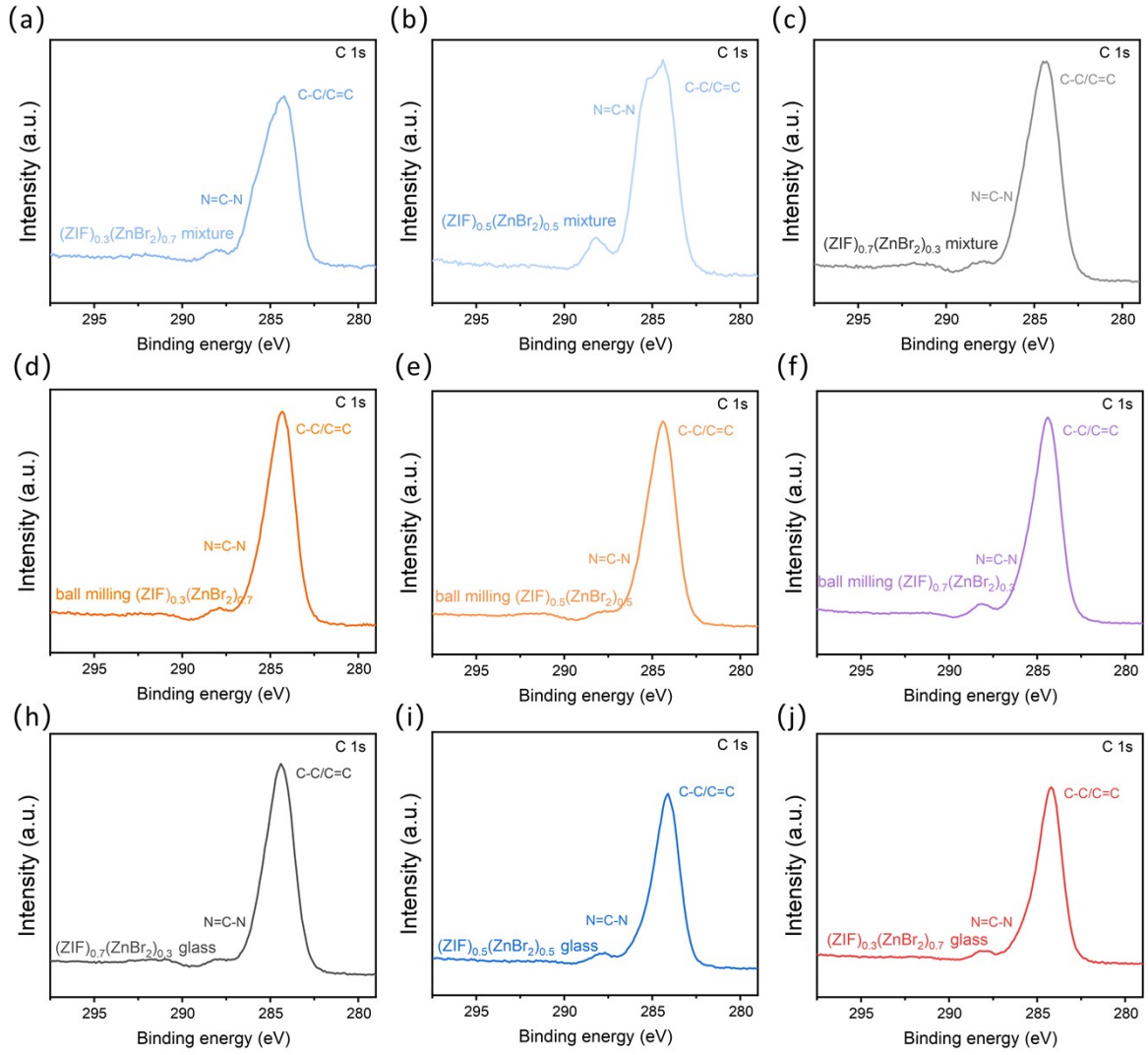

Figure S5. High-resolution C 1s X-ray photoelectron spectroscopy (XPS) spectra of samples in different processing states. (a-c) Physical mixtures, (d-f) ball-milled mixtures, and (g-j) melt-quenched hybrid glasses with x=0.3, 0.5 and 0.7. The spectra exhibit characteristic components corresponding to C-C/C=C and N=C-N bonding environments.

Sample	Path	CN[a]	R(Å)[b]	σ^2(Å^2)[c]	ΔE_0(eV)[d]	R factor
Zn K-edge (S_0^2=0.756)						
Zn foil	Zn-Zn	6.0*	2.638±0.007	0.0107	-1.7±1.3	0.0096
$(ZIF\text{-}62)_{0.5}(ZnBr_2)_{0.5}$ glass	Zn-N	3.2±0.1	1.992±0.008	0.0081	3.6±1.6	0.0072
	Zn-Br	1.0±0.3	2.599*	0.0150	5.0±1.9	
	Zn-C	7.1±1.2	2.975±0.018	0.0081	-6.4±2.6	
	Zn-C/N	6.5±0.7	4.298±0.022	0.0172	2.8±1.3	
ZIF-62(Zn)	Zn-N	4.0±0.1	1.991±0.005	0.0050	6.4±1.2	0.0081
	Zn-C	8.2±1.1	2.964±0.018		-1.1±2.9	
	Zn-C/N	8.4±0.7	4.278±0.017	0.0149	1.8±1.0	

Table S2. Zn K-edge EXAFS fitting parameters of the Zn foil reference, pristine ZIF-62 crystal, and $(ZIF\text{-}62)_{0.5}(ZnBr_2)_{0.5}$ glass. Notes: [a]*CN*, coordination number; [b]*R*, the distance between absorber and backscatter atoms; [c]σ^2, the Debye Waller factor value; [d]ΔE_0, inner potential correction to account for the difference in the inner potential between the sample and the reference compound; R factor indicates the goodness of the fit. $S0^2$ was fixed to 0.756, according to the experimental EXAFS fit of Zn foil by fixing *CN* as the known crystallographic value. * This value was fixed during EXAFS fitting, based on the known structure of Zn. Fitting conditions: *k* range：3.0-11.5; R range: 1.0-4.0; fitting space: *R* space; *k*-weight = 3. A reasonable range of EXAFS fitting parameters: $0.700 < S0^2 < 1.000$; $CN > 0$; $\sigma^2 > 0$ Å2; $|\Delta E_0| < 15$ eV; R factor < 0.02.

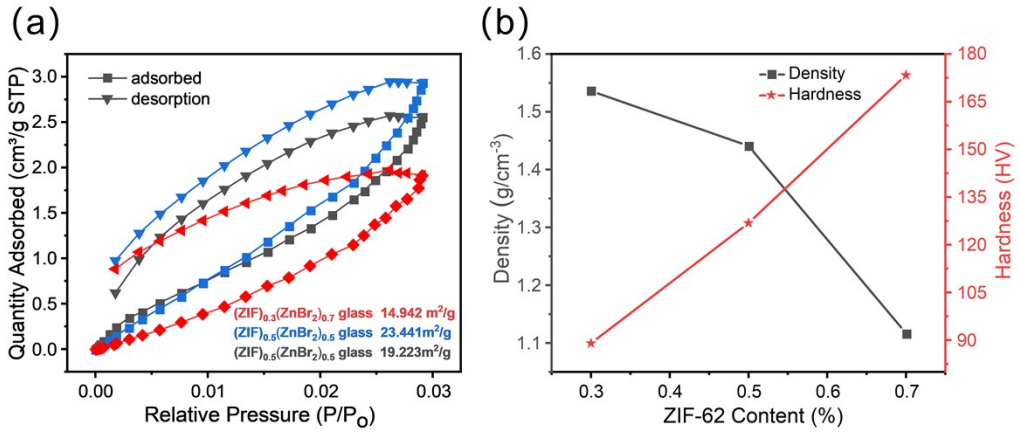

Figure S6. Porosity and mechanical properties of hybrid glasses. (a) CO_2 adsorption-desorption isotherms measured for different glass compositions, with the corresponding BET surface areas indicated. (b) Density (black squares) and Vickers hardness (red stars) as a function of ZIF-62 content.

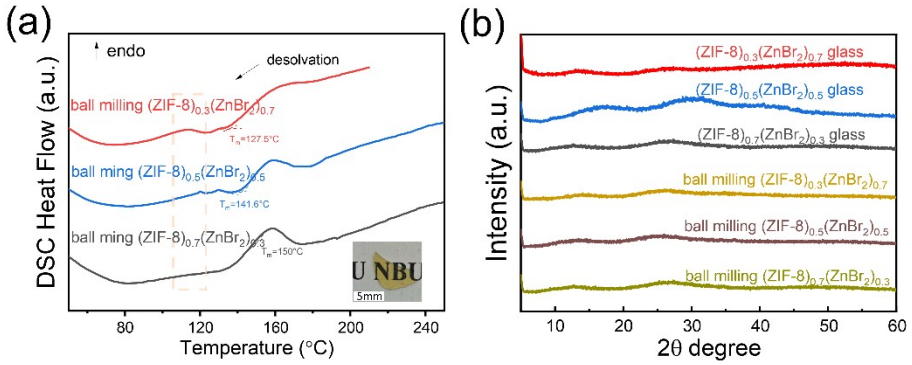

Figure S7. a Thermal melting behavior of the ZIF-8/$ZnBr_2$ hybrids (inset: photographs of the glass samples). **b** XRD patterns of hybrid amorphous ZIF phases, and ZIF-8/$ZnBr_2$ hybrid glasses, further verifying amorphization after ball milling and successful glass formation via hot-pressing.

Reference

1. T. D. Bennett, Y. Yue, P. Li, A. Qiao, H. Tao, N. G. Greaves, T. Richards, G. I. Lampronti, S. A. T. Redfern, F. Blanc, O. K. Farha, J. T. Hupp, A. K. Cheetham and D. A. Keen, *Journal of the American Chemical Society Melt-Quenched Glasses of Metal–Organic Frameworks*, 2016, 138, 3484-3492.
2. L. Frentzel-Beyme, M. Kloß, P. Kolodzeiski, R. Pallach and S. Henke, *Journal of the American Chemical Society Meltable Mixed-Linker Zeolitic Imidazolate Frameworks and Their Microporous Glasses: From Melting Point Engineering to Selective Hydrocarbon Sorption*, 2019, 141, 12362-12371.
3. V. M. Fokin, M. L. F. Nascimento and E. D. Zanotto, *Journal of Non-Crystalline Solids Correlation between maximum crystal growth rate and glass transition temperature of silicate glasses*, 2005, 351, 789-794.
4. L. Tichý and H. Tichá, *Journal of Non-Crystalline Solids Covalent bond approach to the glass-transition temperature of chalcogenide glasses*, 1995, 189, 141-146.
5. J. Hajtó and T. Kemény, *Journal of thermal analysis Thermodynamic data on chalcogenide glasses*, 1976, 9, 53-58.
6. W. Tu, X. Li, Z. Chen, Y. D. Liu, M. Labardi, S. Capaccioli, M. Paluch and L.-M. Wang, *The Journal of Chemical Physics Glass formability in medium-sized molecular systems/pharmaceuticals. I. Thermodynamics vs. kinetics*, 2016, 144.
7. H. F. Hu, Ma, F. D., & Mackenzie, J. D. , *Journal of the Chinese Ceramic Society New Halide Glasses—Zinc Bromide-Based Glasses*, 1984.
8. C. A. Angell and J. Wong, *The Journal of Chemical Physics Structure and Glass Transition Thermodynamics of Liquid Zinc Chloride from Far-Infrared, Raman, and Probe Ion Electronic and Vibrational Spectra*, 1970, 53, 2053-2066.